# Characterizing Brain Mechanics during a Two-Phase Response to Dynamic Overpressure Loading

A. C. Merkle, R. A. Armiger, K. A. Ott, A. C. Wickwire,
A. S. Iwaskiw, L. M. Voo, and C. M. Carneal

## ABSTRACT

*Over the last decade, blast-induced Traumatic Brain Injury (bTBI) research on both animal and computational models has largely focused on investigating injury mechanisms due to overpressure. However, more recent efforts have demonstrated that primary blast loading results in a two-phased response: a short (~1 ms) kinetic event followed by a much longer duration (~300 ms) kinematic response. The characterization of this two-phase response suggests that multiple injury mechanisms in the brain, including early phase stress and later phase strain, should be considered when studying bTBI. Experimental characterization of these responses provides data needed for validating computational models and elucidates each response's potential mechanistic contribution to injury outcomes. The objective of this effort was to characterize both the intracranial pressure response and relative brain displacement due to dynamic overpressure loading conditions that may correlate to bTBIs. A series of shock tube tests were performed on the head-neck complex of a post mortem human surrogate (PMHS) to simulate exposure to blast loading. The overpressure dose applied to the specimen was measured using a sensor affixed to the anterior skull while the pressure transmitted through the skull was collected at four locations within the cranial cavity. Four columns of radiopaque displacement markers were implanted into the brain and tracked using a custom-developed high-speed cineradiography system to provide local brain tissue displacement. The resulting intracranial pressure and brain displacement data collected confirmed the presence of a two-phase response. The pressures were found to initiate and subside within 10 ms of the incident pressure imparted to the PMHS. Peak pressure transmission into the skull was less than 20% of the incident pressure applied to the specimen. This loading resulted in global head motion and subsequent brain motion. The brain motion occurred over a 300 ms duration and excursions ranged from 1.9 - 13.4 mm. These data are being used to describe the mechanics of brain response during overpressure loading and to validate the predicted response from a detailed head-neck finite element model. Further experimental studies will be performed to capture the effect of head-neck orientation and secondary blunt impact.*

# INTRODUCTION

**T**raumatic brain injuries (TBIs) pose a serious, long-term public health issue. The Centers for Disease Control estimate that 1.7 million civilians suffer traumatic brain injuries each year, primarily from head impacts due to falls and motor vehicle accidents (Faul, 2010). Additional studies suggest that TBIs may be underreported, especially in sports head impacts, and may actually be closer to 3.8 million occurrences each year (Langlois, 2006). The Department of Defense has documented more than 253,000 cases of Traumatic Brain Injury (TBI) among service men and women since 2000 (MHS, 2013). For the military subset of TBI injuries, a review of casualties in Afghanistan and Iraq from 2001 to 2007 found that explosions were associated with 63% of all TBI diagnoses (Wojcik, 2010) and a similar study of U.S. Navy and Marine Corps casualties in Iraq during 2004 found that explosions were associated with 52% of all TBI cases (Galarneau 2008). Therefore, although the precise etiology remains in question, there is evidence supporting TBI generated as a result of exposure to explosive events, termed blast-induced TBI (bTBI).

Head injury mechanisms have typically been attributed to either a direct impact or a rapid head acceleration or deceleration. However, over the last decade, bTBI research on both animal and computational models has largely focused on investigating injury mechanisms due to overpressure. In a primary blast loading environment, the object exposed to the blast experiences a short duration, large magnitude rise in overpressure generated by the shockwave. Once the initial loading is complete, the object will move based on the nature of the impulse applied to the surface geometry and the characteristics of the pressure profile. This two-phase response to blast loading (Merkle, 2009) involves what the authors have termed a Kinetic and a Kinematic phase. Human head and neck surrogates exposed to live-fire blast testing demonstrated that the Kinetic phase notionally lasts less than 10 milliseconds and is characterized by large linear accelerations and a rise in intracranial pressure (ICP), but limited head/brain motion. However, the Kinematic phase is a longer duration response (100s of milliseconds) and includes global head motion, ultimately leading to relative motion of the brain with respect to the skull (Merkle, 2012a). Both the short duration change in ICP and the motion-induced strains in the brain are assumed to be biomechanical correlates to bTBI.

An extensive amount of research has been conducted for traditional head injury mechanisms due to blunt trauma or inertial loading (Meaney, 2011, King, 2003). Direct impacts to the head have largely been described based on linear acceleration measurements which correlate to skull fracture and focal brain injuries (Gurdjian, 1950). Computational head modeling of blunt impact events has shown that the linear acceleration response correlates well with increases in brain pressure (Zhang, 2004). Inertial loading scenarios on animal models have demonstrated that angular acceleration without head contact may produce both focal and diffuse brain injuries (Gennarelli, 1982). Therefore, with both the impact due to the applied shock loads as well the resulting motion that occurs due to blast, both injury mechanisms should be considered when characterizing the head response and risk of bTBI.

The response of human models, both computational and experimental, has been studied within a blast environment. Human surrogates, including the Hybrid III dummy (Bass, 2005) and the Human Surrogate Head Model (HSHM) (Merkle, 2012b) were used to determine effects of close proximity blast loading on the head. Experiments utilizing the Hybrid III are limited by the system capabilities and have therefore focused on the global head acceleration response and associated injury criteria originally developed for predicting skull fracture. Surrogates such as the HSHM include additional measurement capabilities developed for the blast environment, but there is very limited data to validate the response. The best available source of validation data will likely be generated from post mortem human surrogate (PMHS) tests. To date, the PMHS data currently available either includes very few experiments or includes only short term response (eg., pressure measurements). Therefore, data from PMHS experiments conducted in a blast environment are necessary to first describe the mechanics of the response and then to generate a dataset for validating human surrogate systems. Therefore, the objective of this paper is to describe a protocol used to test PMHS specimen in a blast environment and to report the results from one of the first specimen tested utilizing this protocol.

# METHODS

An experimental protocol was devised for exposing an unconstrained head-neck complex to simulated blast loading. This protocol required the use of perfused fresh-frozen PMHS specimen.

## Specimen Preparation

Specimens were obtained from the Maryland State Anatomy Board. The specimen referenced in this manuscript included the head and neck sectioned between the sixth and seventh cervical vertebra. Pre-test computed tomography (CT) scans were taken of each specimen at the Johns Hopkins University Medical Institute Radiology Department. Details of the specimen tested for the experiments discussed in this paper are provided in Table 1.

Table 1. Specimen Details.

| Specimen: APL 12-0248 | |
| --- | --- |
| Race | Caucasian |
| Cause of Death | Liver Cancer |
| Age | 63 |
| Weight (kg) | 84 |
| Height (cm) | 175 |
| L1-L4 BMD (g/cm$^2$) | 1.168 |

The jaw was mechanically secured to the maxilla through a series of screws implanted into the bone. Orthopedic wire was laced between each anchor point to prevent the jaw from opening during a test. In preparation for perfusion with artificial cerebrospinal fluid (aCSF), the common carotid arteries, internal jugular veins, and spinal dura were isolated. The exposed end of the spinal dura was dissected to separate the spinal cord and dural sheath. At least 1 cm of the spinal cord was then excised. Barbed fittings were attached to the isolated vessels and dural sheath and secured with sutures. Soft tissue, other than spinal ligaments and vasculature, were dissected away up to the level of the fourth cervical vertebrae. Tubing was attached to each of the fittings to setup flow for perfusion.

To rigidly pot the specimen, Steinman pins were placed bilaterally into the second and third vertebral body to provide additional mechanical purchase. The dissected neck was positioned inside of a 10 cm collar and secured with polymethyl-methacrylate. A custom fixture was utilized to suspend the head while aligning the neck within the collar. The vasculature, with fittings and tubing, were not captured within the potting.

## Specimen Instrumentation

The specimen was instrumented to measure head kinematics, surface and intracranial pressures, and skull strain. Brain displacement was measured using the combination of implanted markers and cineradiography tracking techniques. Local skull deformations were measured by a series of four strain gauge rosettes (C2A-06-125WW-350 Stacked Rosette Gages, Micro-Measurements) mounted to the bone surface on the left skull hemisphere at four locations: the frontal, parietal, temporal, and occipital bones. To place the gages, approximately 1 x 2 cm sections of scalp were elevated to create flap The exposed bone was

prepared by cleaning and abrading the surface, then sequentially applying a conditioner and neutralizer. M-Bond adhesive was applied to both sides of the strain gauge rosette. A small square of a medical examination glove was cut out and placed on the top of the rosette whereby it was pressed onto the prepared bone surface. A small piece of butyl rubber was adhered to the gages to provide a moisture-tight seal and to protect the gages during the experimentation.

Anterior pressure loading was measured using a pressure transducer affixed to the specimen face. A small region of soft tissue was excised from the inferior aspect of the frontal bone at the glabella at which time the exposed bone was cleaned and lightly abraded. A flat-profile pressure transducer (8515CM35-502, Endevco Inc.) was adhered with cyanoacrylate. Intracranial pressures were measured at multiple locations within the skull cavity (8510C-50, Endevco Inc.). Four locations on the right half of the skull (mirrored to those of the strain gauges on the left side of the skull, as shown in Figure 1) were drilled and tapped to create ports for each pressure sensor. To avoid protruding beyond the skull and into the brain, the thickness of the skull at the installation locations was determined from the CT scan. The transducer stand-off was then customized to allow the sensing face to sit flush with the inner skull surface, but within the dura. An O-ring was included to seal the installation site.

Within the brain, radiopaque displacement markers (RDMs) were carefully staged and suspended within the biosimulant. These were 2.4 mm diameter spheres of open cell foam coated in radiopaque ink for an effective density of 2.11 g/cm$^3$. The markers were aligned in four columns in the sagittal plan. The two most anterior columns (A, B) consisted of six markers whereas the posterior columns (C, D) had as many as seven markers each. The locations of the markers are illustrated in Figure 1.

Insertion of the RDMs into the intact brain was achieved via a transcranial cannula. The target locations were identified for the native brain by mapping the specified location of the markers to the external skull surface. A surgical plan for RDM installation was developed using an optical tracking system (Polaris, Northern Digital Inc.) and custom software, developed by JHU/APL, to stereotactiacally monitor the position and orientation of surgical instruments in real-time. Markers were inserted through the hole of the cannula and then guided to the tip via a push rod. In each case after an RDM was inserted, the cannula was withdrawn to a distance defined in the preoperative plan to the next insertion site. After completing each column of RDMs, the access holes were re-sealed with a 0.25 inch screw outfitted with an O-ring.
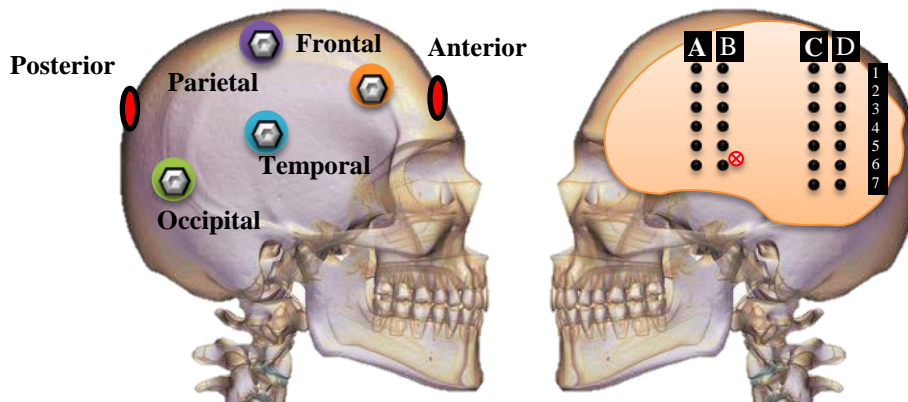


Figure 1. Sensor placement of the pressure transducers (left) and radiopaque displacement markers (RDMs) (right). The pressure transducers were implanted at the same location as the strain gages but on the contralateral side.

## Test Configuration

The instrumented specimen was placed in an inverted configuration and gripped by the potting fixture attached to the cervical spine. The specimen was positioned directly in front of a custom-built, 15 cm diameter shock tube (Cernak, 2011) and between the generator and intensifier of a custom-integrated high-speed cine-radiography system (HSXR) as shown in Figure 2. The HSXR is comprised of an x-ray generator, a 41-cm image detection unit, and a high-speed digital video camera to operate in synchronization.

The nose of the inverted specimen was centered on the shock tube and placed approximately 15 cm from the tube opening. All tests covered in this manuscript are for forward facing configurations where the incident pressure wave first impacts the nose of the specimen. Vertical and horizontal alignment measurements were recorded relative to the HSXR and shock tube systems. The perfusion was then performed using an in-line gravity feed of aCSF.

## Data Collection and Processing

Tests were conducted with nominal driver pressures of 425, 550 and 700 kPa. Data from the specimen's instrumentation suite was collected at a rate of 1 megasample per second (Dewetron Orion, Dewetron, Inc.) with a 300 kHz hardware anti-alias filter applied. Collected measurements included: three-dimensional head/neck kinematics, brain displacement at 26 locations, surface skull strain at 4 locations and ICP responses at the epidural layer. Post-test CTs were collected after completing the test series to compare with pre-test CT datasets for any sustained injury. Pressure data was then processed using Matlab (Matlab R2013b), removing any signal offset and then applying a 15 kHz low pass filter to the internal pressure results. This filter frequency was chosen after review of the frequency spectrum of the internal pressure results indicated the response to be below this frequency level. Surface pressure data was not filtered during post processing.

Data from the HSXR was used to measure brain displacement. In high-speed dynamic event capture, an Anatomically Programmed High Frequency X-ray Generator (CPI Indico 100) provided a continuous, non-gated beam using 75-200 mA and 70-105 kVp settings. The image detection unit (Thales TH 9447 QX) included an output phosphor capable of a 3 kHz response. A high-speed video camera (Phantom v10, Vision Research), operating at 480 frames per second in synchronization with the x-ray source and shock tube event, was used to record the images from the output of the image detection unit.

A series of image processing steps was needed in order to extract and determine brain marker displacement relative to the skull. First, the acquired x-ray images were rectified and dewarped using a custom-built imaging phantom with a regularly spaced group of markers. A 2D-3D registration algorithm was used to localize the skull in each dewarped frame. The registration algorithms use the post-test CT scan as a reference to generate digitally reconstructed radiographs (DRR) from an assumed source location. The DRR is compared to the actual radiograph by means of a GPU-accelerated optimization algorithm that updates the source location. By comparing gradient information, the solution converges to a point that best represents the true source location with respect the skull.

Using the dewarped x-ray frames and the localized skull, the image was prepared for segmentation by applying a lowpass Gaussian filter with kernel size of 45 pixels and sigma equal to 35. This heavily blurred image was then subtracted from the original. The resulting image was then filtered again using a 12th order finite impulse response filter with a normalized cutoff frequency of 0.001. The brain markers were then localized using a modified hough transform for circles. The segmented markers were then tracked across subsequent frames while being identified from the previous frame based on a minimum distance between the solved marker location for the previous frame and the current frame.
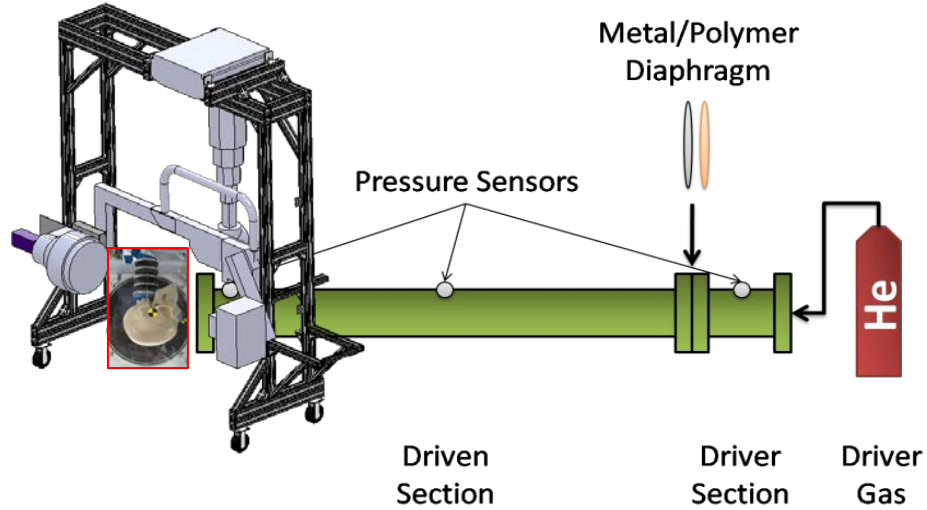
Figure 2. Schematic showing the general test setup for the shock tube, inverted head-neck specimen and high-speed x-ray system.

## RESULTS

The results presented in this paper will focus on those recorded from a single specimen (APL-12-0248) tested at nominal shock tube driver burst pressures of 425, 550 and 700 kPa. Specifically, this preliminary reporting and analyses will focus on the recorded pressure measurements and brain displacements. The test matrix consisted of the three driver pressure levels, with each condition repeated once (Table 2). The peak pressure measured on the surface of the specimen as well as at each location within the skull is provided for each experiment. A representative pressure-time history for the surface and intracranial pressure response is shown in Figure 3. The peak overpressure from each ICP sensor was plotted against driver pressure for all tests to provide a sensitivity of each pressure response to loading conditions (Figure 4).

6

Table 2. Intracranial Pressure Results for Specimen APL-12-0248.

| Test Number | Driver Pressure (kPa) | Peak Surface Pressure (kPa) | Peak Intracranial Pressure (kPa) | | | |
|---|---|---|---|---|---|---|
| | | Anterior | Frontal | Parietal | Temporal | Occipital |
| 1 | 422.8 | 250.8 | 9.8 | 5.7 | 32.5 | 13.8 |
| 2 | 549.6 | --* | 11.7 | 9.1 | 45.9 | 12.5 |
| 3 | 428.4 | 255.4 | 10.4 | 8.3 | 32.8 | 12.4 |
| 4 | 548.4 | --* | 13.4 | 9.3 | 47.3 | 15.9 |
| 5 | 718.6 | --* | 17.4 | 9.5 | 58.2 | 15.0 |
| 6 | 706.9 | --* | 18.0 | 13.9 | 60.4 | 18.2 |

* Although the surface pressure sensor had some functionality during these tests, the measurements were compromised due to fluids and intermittent response.
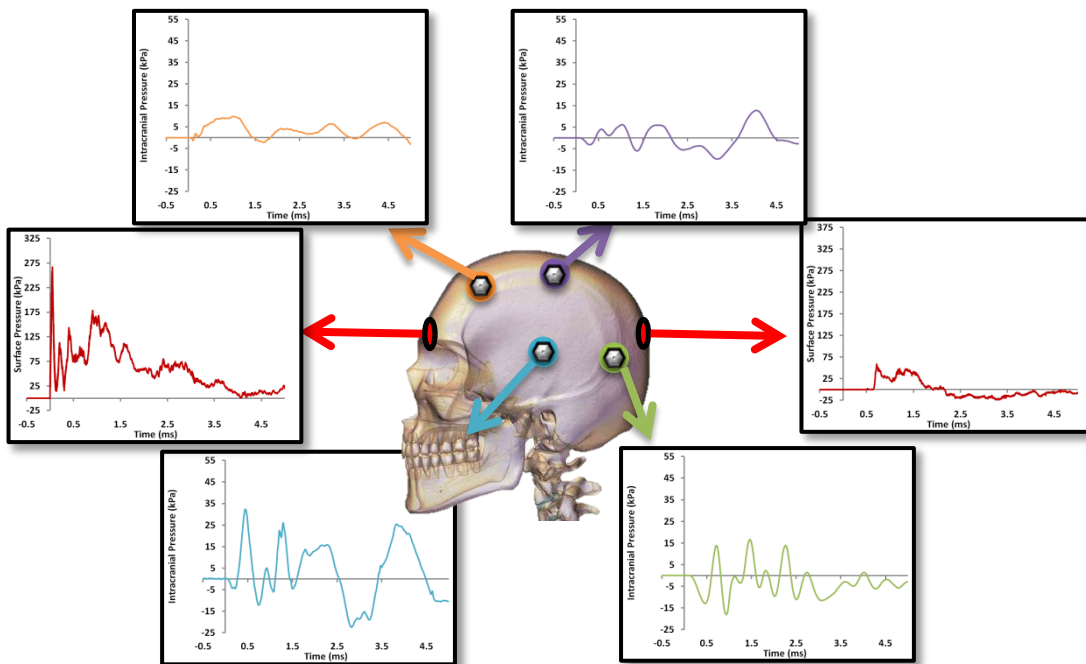


Figure 3. Recorded pressure signatures from surface and intracranial pressure sensors for a 550 kPa shock tube driver pressure (Test 1).
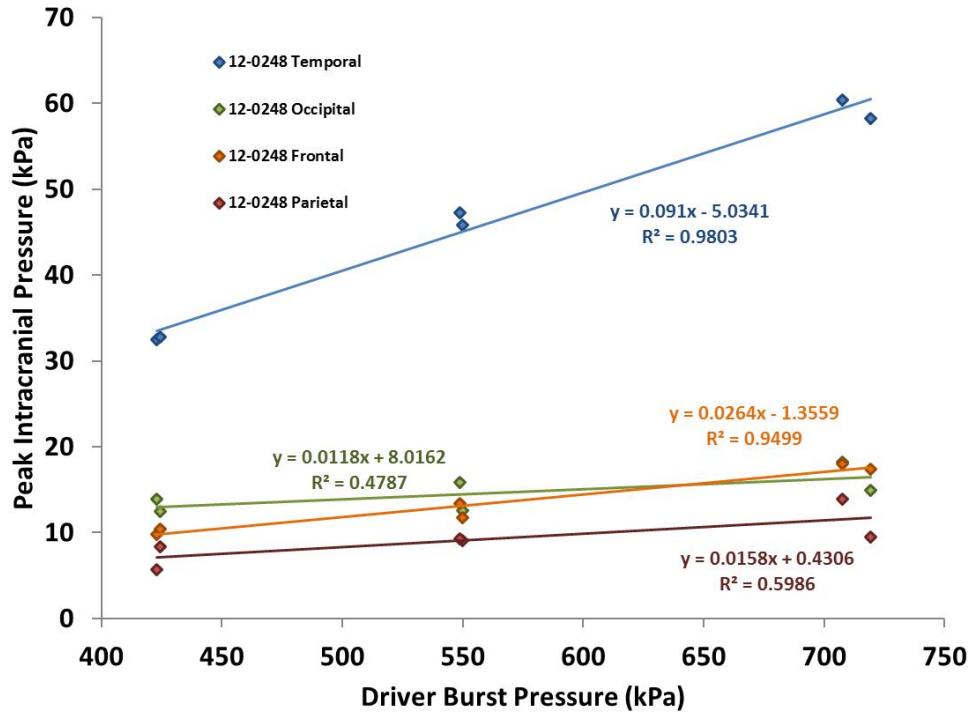
Figure 4. Trends relating the response of peak intracranial pressures with respect to driver burst pressure.

The motion of each implanted RDM was tracked optically using the methods discussed above. For a 550 kPa driver pressure, the displacement in the X and Z directions are shown in Figure 5 for a single RDM at location A6. The local coordinate frame for the skull, which determines polarity for brain displacements, was defined with the origin on the midsagittal plane, between the left and right auditory meatuses. The X axis was defined by the Frankfort plane with positive moving from posterior to anterior. The Z axis was defined from the same origin with positive direction moving from the cranial to caudal direction. The spatial response for each RDM is traced in Figure 6 and overlaid on the actual image of the specimen. Columns C and D have less tracked markers than planned due to markers that migrated away from their installation point either prior to or during the testing sequence. This is largely attributed to implantation locations that encountered the ventricles. Using the tracked data, the maximum excursion, defined as the straight line distance between the furthest most (X, Z) displacements for a given marker, was determined. These excursions were averaged for the two tests performed at each driver pressure level to determine a mean response. The individual values and the average excursion for the markers from columns B and D for Test 2 and Test 4, both targeting a 550 kPa driver pressure, are provided in Table 3.
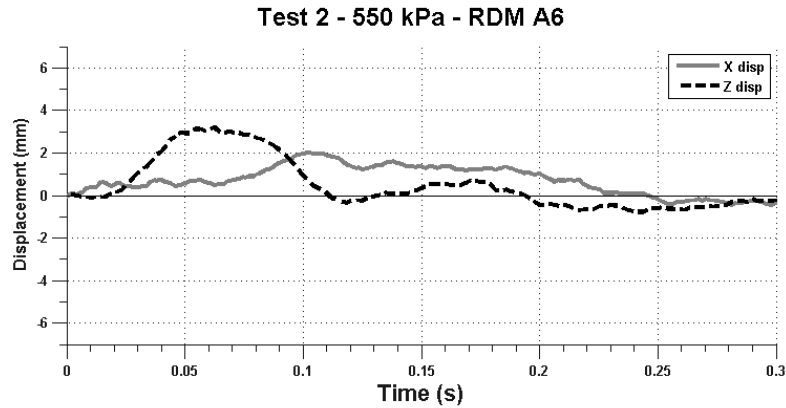
Figure 5. Displacement (X and Z) plotted against time for the A6 radiopaque displacement marker for Test 2. The spatial plots are overlayed on the actual starting locations of the markers in the initial HSXR image.
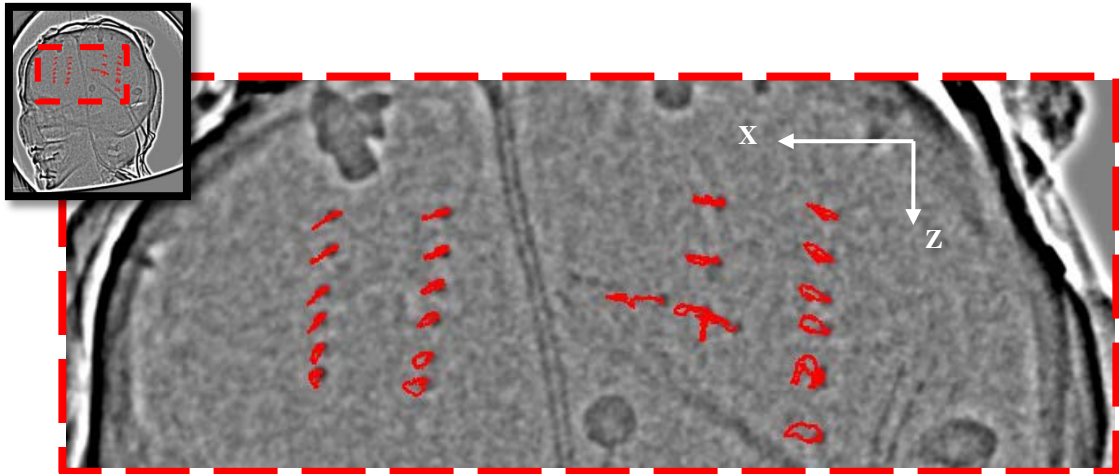


Figure 6. Response of brain displacement markers during a 550 kPa test.

## DISCUSSION

### Pressure Response

PMHS response initiates with the arrival of pressure at the front surface mounted pressure sensor. The ICP response is observed to begin within 0.2 ms of the arrival of the pressure to the skull. Any appreciable overpressure is gone within 5 ms of the beginning of the event (Figure 3). The observed peak pressures occur within 1 ms of the initial surface pressure arrival for all pressure sensor locations. However, the pressure-time history is extremely dependent upon the sensor location. For example, Test 1 shows that pressure measured within the cranium near the frontal bone is the first to respond and has a positive pressure rise. The overpressure peak of 9.8 kPa occurs at 1 ms and maintains a positive duration for approximately 1 ms. The sensor mounted to the parietal bone is located in the upper regions of the cranium but posterior of the frontal bone sensor. The response at this location actually shows an initial negative pressure response followed by a positive overpressure. The sensor mounted to the temporal bone is located inferior and lateral to the sensors

9

mounted to the frontal and parietal bones. The temporal sensor response indicates a small negative pressure followed by a comparatively large positive overpressure. The fourth ICP sensor was mounted to the occipital bone at a location posterior to all other sensors and inferior to the parietal and frontal sensors. With close proximity to the back of the skull, this location provided the most pronounced negative pressure response followed by a positive overpressure and secondary oscillations.

Table 3. Peak Brain Radiopaque Displacement Marker Excursion for Specimen APL-HH12-0248 for the 550 kPa Driver Pressure.

| Radiopaque Displacement Marker Excursion (mm) | | | | | | |
|---|---|---|---|---|---|---|
| Row | Column B | | | Column D | | |
| | Test 2 | Test 4 | Mean | Test 2 | Test 4 | Mean |
| 1 | 6.7 | 6.7 | 6.7 | 7.7 | 5.7 | 6.7 |
| 2 | 6.3 | 5.9 | 6.1 | 7.9 | 6.5 | 7.2 |
| 3 | 5.8 | 4.9 | 5.3 | 7.9 | 6.4 | 7.1 |
| 4 | 5.4 | 4.0 | 4.7 | 8.1 | 5.8 | 7.0 |
| 5 | 5.5 | 3.9 | 4.7 | 10.4 | 12.1 | 11.2 |
| 6 | 6.6 | 4.7 | 5.7 | 10.4 | 12.1 | 11.2 |
| 7 | -- | -- | -- | 9.8 | 8.2 | 9.0 |

These results demonstrate that the pressure can vary significantly within the brain. Prior modeling efforts using human surrogates and computational models (Roberts, 2012) have shown that the greatest positive pressure occurs at the anterior most locations and that the peaks decrease when measuring from anterior to posterior in the brain. However, these data were all measured at the mid-sagittal plane, thus querying locations embedded deep within the simulated brain tissue. In the experiments presented here, the sensor implantation targeted the sub-arachnoid space at the interface with the brain. Therefore, it is not unexpected to see local anatomy and interfaces influence trends. The greatest pressures were seen at the temporal location due to it being most vertically aligned with the center of the applied load and more rostral than the occipital sensor. The most posterior sensor location (occipital) shows an increase in negative pressure initially, which is the opposite of the frontal sensor. The frontal and occipital internal pressure traces imply a coup-contrecoup response. This effect has been shown to occur in modeling activities and other experimental investigations. Both blunt impacts to the head (Hardy, 2007) and shock tube experiments on PMHS (Bir, 2007) demonstrate a similar mirrored response between the frontal and occipital sensors, with the frontal sensor having a positive initial peak and the occipital sensor showing a negative initial response. The effect is attributed to a combination of factors including an initial response to global acceleration and the potential for cavitation at the contrecoup location. Further experimentation will be used to confirm these trends in additional specimen. Additionally, computational models will be used to study the response differences predicted at locations more closely aligned with the instrumentation chosen in this experimental protocol.

Three nominal test levels, as described by shock tube driver pressure, were used to generate increasing severity pressure levels to the head-neck specimen. Figure 3 provides the effect of driver pressure on intracranial pressure response for all six experiments. For this exposure range, the responses of the most anterior sensors (Frontal and Temporal) are well explained by a linear fit. With only two experiments at each level, some variation is observed in the occipital and parietal responses, which decreases the agreement of the linear trend line and the data. For all responses, an increase in driver burst pressure does create an increase in brain pressure. However, the proportionality of the increase varies. When considering the differences

between the 425 kPa and 700 kPa cases (a 65% increase in nominal peak pressure), the parietal pressure matches most closely with a mean 67% increase. However, the frontal and temporal responses for the same conditions increase by 74% and 84%, respectively. Interestingly, the positive peak pressure for the occipital location increased by only 27%. The occipital location's comparative insensitivity to exposure level could be due to a number of factors. First, there are only two data points for each test level and this location was the least repeatable, therefore more experiments are needed. Second, the occipital location reflected a more significant increase in the negative pressure peak with increased pressure loading to the face. This again suggests that the contrecoup response is being accentuated with increased loading. These results will again be explored with future testing on additional specimen.

The anterior skull surface pressure is a good indicator of the overpressure dose experienced by the specimen. Unfortunately, the sensor was only found to be reliable for two experiments within this test series. This was determined to be due to a combination of fluids (biological and biosimulant fluids) disrupting sensor operation and the sensor becoming dislodged from its mounting point during testing. The anterior surface sensor did perform well for both 425 kPa driver pressure tests, Tests 1 and 3, and measured 250.8 and 255.4 kPa, respectively. The temporal pressure response for these tests, with peaks of 32.5 and 32.8 kPa, reflect a greater than 85% reduction between pressure measured external to the skull and within the brain. This signal attenuation is predominantly attributed to transmission losses as the pressure wave propagates through the skull and the sinuses. The amount of pressure transmitted through the skull as a result of overpressure loading has been studied in animals and human surrogates (Chavko et al., 2007, Saljo et. al, 2008, Merkle et al., 2010, Shridharani, 2012). While the transmitted component has ranged, attributed to differences in experimental setup and data types presented, those studies actually reporting a reflected surface pressure do show a decrease in for intracranial pressure as compared to surface pressure. Specifically, animal models (Saljo et al., 2008) were developed for rat and pig exposed to shock tube loading. The pig model showed a 41.5% average peak air pressure with respect to intracranial pressure, while the rat model was 90% of the pressure measured in the surrounding air. Chavko et al. [21] noted that only a small part of the blast wave is absorbed by the rat skull during shock tube loading. These findings imply the properties of the skull, and likely additional anatomical features such as sinuses, have a large effect on the transmission of pressure into the brain. This helps to explain the significant drop in pressure for the intracranial pressures measured in this experiment.

## Brain Displacement Response

Brain displacement occurs over a much longer time duration than what was observed from the pressure response. Figure 5 shows that while some small amount of marker displacement does occur within the first 10 ms, peak displacements do not occur until well after 50 ms with a measurable response beyond 300 ms after the pressure wave initially loads the specimen. This longer duration brain motion phase confirms similar observations made in human head surrogates and computational models (Merkle, 2012, Roberts, 2012). For the A6 RDM, located forward and slightly above the estimated head center of gravity, motion initially occurs toward the face (+X) and downward (+Z). By 60 ms, the RDM reaches a peak of 3 mm of displacement downward while it continues to move forward in the X direction until reaching a peak of 2 mm at 100 ms. The mean peak excursion for the A6 RDM for the 550 kPa shock tube driver pressure was 5.7 mm. By 300 ms, the A6 RDM returned to its origin.

The displacement vector for each RDM is governed by the global motion incurred by the skull and the marker's location within the brain. For these tests, the anterior facial pressure loading created by the shock tube results in a combination of rearward head translation and rotation (due to neck extension). The brain initially lags this skull motion resulting in an opposite "rotation" with respect to the skull. Figure 6 confirms the brain rotation as the trace for each RDM shows each marker initially displacing to the left and either moving up or down dependent upon its location with respect to the center of rotation. The RDMs in Column A move forward and downward while those in Column D move forward and upward before returning to their origin. Furthermore, Figure 6 shows that the superior rows (1-3) for each RDM column form a very narrow band of movement and effectively trace a line. However, the more inferior rows (4-6) travel in a path that shows more of an elliptical shape. This difference could be in part due to the additional brain structures, including the corpus callosum, that lie closer to the more inferior columns and may affect the local motion.

It is believed that this manuscript is the first to report tracking of brain motion in PMHS during overpressure loading representative of blast. The RDM excursions for these tests ranged from 4-12 mm. It is yet unknown as to the magnitude of strain endured by the local tissues due to this loading. Once known, these values could contribute to assessing the risk of brain injury due to existing strain based criteria. With no other data yet available for comparison in the blast loading regime, comparisons were made to data generated from blunt impact conditions used to model automotive impact conditions (Hardy et al., 2007). For those studies, head impacts of various magnitudes and with/without head protection were conducted. The results showed maximum average excursions that ranged from 1.9 to 13.4 mm. While the specific RDM motion is highly dependent on the loading and the position of the RDM, the excursions reported by the blunt impact studies are in a range very similar to those reported here. This is important to note because the modeling performed as part of that study suggested that the strain levels obtained were approaching levels deemed to be injurious.

## Limitations

The current manuscript introduces a new protocol for generating and collecting results from six blast-simulated experiments on a single specimen. More experimentation is required to confirm the response trends and findings reported from this initial test series. Future experiments must also resolve challenges incurred with instrumentation, specifically the surface pressure sensors. A reliable surface pressure sensor must be selected and installed in a manner that will ensure durability and repeatable results. The RDM implantation protocol should also be further refined to avoid the ventricles which allow the markers to displace while not coupled with the brain tissue.

## CONCLUSION

This manuscript provides the first ever analysis of intracranial pressure and brain displacement data generated from simulated blast results on PMHS. The results demonstrate an early phase pressure response followed by a longer duration brain motion. This confirms predictions of this multi-phase response from human head surrogates and computational models and will be used as validation data. Additionally, the displacements noted in these non-contact experiments are close in magnitude to those measured during blunt impact testing and subsequently related to axonal strain injury criteria. Now that the protocol has been developed and proven with initial results, additional testing must be performed to confirm the findings presented herein.

## ACKNOWLEDGEMENTS

## REFERENCES

BASS, DAVIS, RAFAELS, K. et al., (2005) A Method for Assessing Blast Protection in Explosive Ordinance Disposal Bomb Suits. Int J Occup Saf Ergon, 347-361

BIR, C. et al., (2007). A Biomechanical Prospective of Blast Injury Neurotrauma RTO-MPHFM-207.

CERNAK I, MERKLE AC, KOLIATSOS VE, BILIK JM, LUONG QT, MAHOTA TM, XU L, SLACK N, WINDLE D, AHMED FA. (2011). The pathobiology of blast injuries and blast-induced neurotrauma as identified using a new experimental model of injury in mice. Neurobiol Dis. 41(2):538-51.

CHAVKO, M. et al., (2007). Measurement of blast wave by a miniature fiber optic pressure transducer in the rat brain. J Neurosci Methods. 159(2): p. 277-81.

FAUL, M. (2010) Traumatic brain injury in the United States: emergency department visits, hospitalizations, and deaths. Centers for Disease Control and Prevention, National Center for Injury Prevention and Control, Atlanta, GA.

GENNARELLI, THIBAULT, HUME et al., (1982) Diffuse Axonal Injury and Traumatic Coma in the Primate. Ann Neurol., 564-574.

GURDJIAN, E.S., WEBSTER, J.E., LISSNER, H.R. (1950). The Mechanism of Skull Fracture. J Neurosurg. 106–14.

HARDY, MASON, FOSTER, SHAH, KOPACZ, YANG, KING, BISHOP, BEY, ANDERST TASHMAN (2007). A Study of the Response of the Human Cadaver Head to Impact. Stapp Car Crash J. 51: 17–80.

KING, Y., ZHANG, H., VIANO D. (2003). Is Head Injury Caused by Linear or Angular Acceleration. International Research Council on Biomechancis of Injury. Lisbon.

LANGLOIS J., Rutland-Brown W., and Wald M. (2006). The Epidemiology and Impact of Traumatic Brain Injury: A Brief Overview. J Head Trauma Rehabil, Vol. 21, No. 5, 375–378.

MEANEY, D.F., AND SMITH, D.H., (2011). Biomechanics of Concussion. Clinics in Sports Medicine. 30.1 19-31.

MEDIAVILLA VARAS, J. et al., (2011) Physics of IED Blast Shock Tube Simulations for mTBI Research. Front Neurol, 2: p. 58.

MERKLE A.C, WING I., ARMIGER, R.A., CARKHUFF B.G., ROBERTS J.C. (2009) Development of a Human Head Physical Surrogate Model for Investigating Blast Injury. in ASME International Mechanical Engineering Congress & Exposition. 2009. Lake Buena Vista, FL

MERKLE A., WICKWIRE A., WING I., CARBONI M., DECRISTOFANO B., MAFFEO M. (2010). Evaluation of the Human Surrogate Torso Model Response to Ideal and Complex Blast Loading Conditions. in Personal Armour Systems Symposium. Quebec City.

MERKLE A., WING I., CARNEAL C. (2012a). The Mechanics of Brain Motion During Free-Field Blast Loading. ASME 2012 Summer Bioengineering Conference. 2012a. Puerto Rico

MERKLE A., WING I. and CARNEAL C. (2012b). Effect of Helmet Systems on the Two-Phased Brain Response to Blast Loading. Personal Armour Survivability Symposium.

MILITARY HEALTH SYSTEM (2013). DoD Worldwide Numbers for Traumatic Brain Injury. Military Health System. Washington, DC.

ROBERTS J. C., HARRIGAN T., WARD E. TAYLOR T., ANNETT M., MERKLE A. (2012). A human head-neck computational model for assessing blast injury. Journal of Biomechanics. 45:2899-2906.

SALJO, A., et al., (2008). Neuropathology and pressure in the pig brain resulting from low impulse noise exposure. J Neurotrauma. 25(12): 1397-406.

SHRIDHARANI, J. K., et al., (2012). Porcine head response to blast. Front Neurol, 3: 70.

WOJCIK, B. E., C. R. STEIN, K. BAGG, et al., (2010). Traumatic Brain Injury Hospitalizations of U.S. Army Soldiers deployed to Afghanistan and Iraq. Am. J. Prev. Med. 38(1):S108–S116.

ZHANG L., Y. K., and KING A., (2004). A Proposed Injury Threshold for Mild Traumatic Brain Injury. J of Biomech Eng. 227-236